Anti-seepage effectiveness evaluation of fracture grouting in Yellow River Embankment

Jian Liu[1], Zhi Wan[1], Quanyi Xie[1], Cong Li[1], Rui Liu[1], Mengying Cheng[1] and Bo Han[1,*]

1 School of Civil Engineering, Shandong University, 17922, Jingshi Road., Jinan 250061,China;
liujianshanda@163.com(J.L.);mscj521@163.com(Z.W.);quanyixiesdu@163.com(Q.X.);licon7@126.com(C. L.);
sdhzjclr@163.com(R.L.); cicmying@yahoo.com(M.C.)

* Correspondence: bo.han@sdu.edu.cn(B.H.); Tel.: +86-531-88396007(B.H.)

Abstract：Fracture grouting has been a widely used mitigation measure against seepage in the Yellow River Embankment. However, there is currently a lack of systematic investigation for evaluating the anti-seepage effectiveness of fracture grouting employed in this longest river embankment in China. Therefore, in this work, laboratory and in-situ experiments are carried out for investigating the reinforcement effect of fracture grouting in the Jinan Section of the Yellow River Embankment. In particular, firstly, the laboratory tests concentrate on studying the optimum strength improvement for cement-silicate grout by varying the content of backfilled fly ash and bentonite as admixtures. Flexural strength and Scanning Electron Microscope photographs are investigated for assessing the strength and compactness improvement. Subsequently, based on the obtained optimum admixtures content, in-situ grouting tests are carried out in the Jinan Section of the Yellow River Embankment to evaluate the anti-seepage effectiveness of fracture grouting, where geophysical prospecting and pit prospecting methods are employed. Laboratory results show that, compared with pure cement-silicate grouts, the gelation time of the improved slurry is longer and gelation time increases as fly ash content increases. The optimum mixing proportion of the compound cement-silicate grout is 70% cement, 25% fly ash and 5% bentonite, and the best volume ratio is 2 for the investigated cases. Geophysical prospecting using the Ground Penetrating Radar and High Density Resistivity methods can reflect the anti-seepage effectiveness of fracture grouting on site. It shows that the grouting material mainly flows along the axial direction of the embankment. The treatment that is used to generate directional fracture is proved to be effective. The injection hole interval distance is suggested to be 1.2 m, where the lapping effect of the grouting veins is relatively significant. For the investigated cases, the average thickness of the grouting veins is approximately 6.0 cm and the corresponding permeability coefficient is averagely 1.6×10^{-6} cm/s, which meets the anti-seepage criterion in practice.

Keywords: fracture grouting, cement-silicate grout, geophysical prospecting, seepage, Yellow River Embankment

1 Introduction

The Yellow River Embankment is the longest river embankment in China, which is mainly constructed with Yellow River alluvial soils, i.e. silt with low surface strength, high porosity and drastic capillarity. Seepage-induced instabilities, such as infiltration, piping and leakage, frequently occurred in the Yellow River Embankment during its long-term operation period, due to its the unfavorable soil properties. Among the potential seepage control methods, fracture grouting has been developing rapidly recently due to its low cost and high efficiency. According to statistics, more than 3000 dangerous reservoirs and 2000km embankments have been reinforced with fracture grouting in the past 20 years.

Researchers have carried out a series of studies on grouting materials [1-3], grouting mechanism and diffusion evolution against seepage through indoor experiments and theoretical analysis. In particular, Warner et al. [4] used compaction grouting to mitigate the sinkholes at WAC Bennett dam,

showing satisfactory reinforcement effect. Grotenhuis [5] predicted the fracture length and thickness of grouting in sandy soil through analytical solutions. Tunçdemir et al. [6] investigated fracture grouting in fissured Ankara Clay with low viscosity cement grouts, where the effect of water/solid ratio and the applied vertical stress on fracturing pressure was studied. Bezuijen [7] studied fracture grouting in sand by developing a conceptual and analytical model and obtained the relationship between crack dimensions and grouting material properties. Yoneyama et al. [8] discussed the mechanism how cement grout controlled water permeation through the fractures in rocks, focusing on the effectiveness of the clogging of cement particles for closing water paths. Yun et al. [9] studied the injection process of fracture grouting and proposed an analytical solution to determine fracture pressure, length and thickness. Wang et al. [10] performed laboratory tests on loose sand under confined boundary conditions to explore the grouting evolution and diffusion process, with different grout water cement ratio and degree of saturation of soil. They highlighted the influence of these two factors on the injected grout volume, grout density and the characteristics of the grouted bulbs. Sun [11] put forward the important factors affecting diffusion radius (i.e. fracture pressure, fracture width, grouting flow et al) and derived the calculation formula of fracture grouting diffusion radius based on the assumption that the soil is isotropic and the calculate model is an ideal parallel plane model. However, those introduced works concentrate on investigating grouting in sand or some specific soil, whose engineering properties are very different from the Yellow River silt. Therefore, the grouting parameters in existing studies cannot be directly used to investigate the anti-seepage grouting in the Yellow River Embankment. Furthermore, due to the complexity and randomness of grouting mechanism and material properties, there is a need for a systematic assessment for the grouting effectiveness in the Yellow River Embankment.

In existing studies, experimental or theoretical works have been conducted to investigate the properties of the Yellow River silt. In particular, Liu et al. [12] established the stress-strain behavior of the Yellow River silt under dynamic loading through dynamic triaxial and resonance column tests. Xiao et al. [13] investigated the basic physic-mechanical properties of the Yellow River silt by a series of laboratory experiments to evaluate and treat the distress of silt rainfall of the Beijing-Jiulong railway in the Yellow River alluvial plain area. Song et al. [14] simulated the rainfall infiltration and capillary rising through laboratory tests and analyzed the hydrophilic characteristics of silty roadbed in the Yellow River alluvial plain. Zhu et al. [15] studied the attenuation law of strength and stiffness of silty embankment under the action of capillary water and the reinforcement effect of the embankment by using the Soletanche method based on large-scale indoor model tests. Chen et al. [16] carried out a number of triaxial tests with stress-controlled monotonic loading and cyclic loading for the Yellow River silt under the CU condition to investigate the influence of cyclic stress amplitude, confining pressure and the induced pore water pressure on the mechanical behavior of the Yellow River silt. Shi [17] studied the bond performance between polymer anchorage body and silt through ultimate pullout tests on vertical polymer anchors. It is noted that the existing studies concentrate on investigating the mechanical properties of the Yellow River silt through indoor tests. However, laboratory tests cannot reflect the in-situ state of soil or reveal realistically the grouting mechanism of fracture grouting in the Yellow River Embankment.

Therefore, in this work, laboratory and in-situ experiments are carried out to investigate the reinforcement effect of fracture grouting in the Jinan Section of the Yellow River Embankment. In particular, firstly, the laboratory tests concentrate on studying the optimum strength and compactness improvement for cement-silicate grout by varying the content of backfilled fly ash and bentonite as admixtures. Flexural strength and Scanning Electron Microscope photographs are investigated for assessing the strength and compactness improvement. Subsequently, based on the obtained optimum admixtures content, in-situ grouting tests are carried out in the Jinan Section of the Yellow River Embankment to evaluate the anti-seepage effectiveness of fracture grouting, where geophysical prospecting and pit prospecting methods are employed. The work provides references for determining the technical construction parameters of practical fracture grouting in river embankment, i.e. distance of grouting holes, the optimum mixing proportion of grouting material and termination condition.

2 Experimental scheme and testing procedure

2.1 Grouting material laboratory experiment

Grouting effectiveness depends on the different materials used in practice. Cement-silicate grout has been widely used due to its short gelation time and high stone rate. However, it has some limitations, such as low-level stability and fluidity, which has restricted its further development. Therefore, experiments are designed to investigate the improvements on the reinforcement effect of the existing cement-silicate grout aiming for the optimum content of backfilled fly ash and bentonite as water reducing agent and expansive agent respectively.

2.1.1 Raw material

The cement used in the experiment is a Portland cement (PC) graded 42.5 and produced by Sunnsy Group in Jinan. The fly ash (FA) can be classified as Class F according to ASTM C618-05 [18]. The compositions of PC and FA are shown in Table 1.The main characteristics and properties of Bentonite (B) is shown in Table 2. The Baume degree and modulus of the silicate are 40 and 3.3 respectively.

Table 1. Main chemical composition of PC and FA

Material	CaO (%)	SiO_2 (%)	Al_2O_3 (%)	Fe_2O_3 (%)
PC	62.60	22.61	4.35	2.46
FA	3.75	54.64	28.09	6.20

Table 2. Main characteristics and properties of Bentonite and silicate

Water absorption	Swell volume	Colloid valence	Particle size (75μm)	Water content
420% (2h)	49ml/g	630ml/15g	95%	9%

2.1.2 Experimental scheme

To improve the grouting effects of cement-silicate grout, fly ash and bentonite are added as admixtures. In particular, first, construction cost can decrease when partially replacing cement with fly ash. Second, the fluidity of grout increases as fly ash particle is sphere and finer. Last but not the least, secondary reaction can occur between fly ash and the reactants of hydration action of cement, and low calcium hydrates like $CaSiO_3$ can be generated, which improves the anti-aqueous solubility of the concretion and promotes the durability of the anti-seepage curtain. According to Sha [19], the optimum percentage of fly ash ranges from 20% to 30%.

Bentonite can improve stability and infiltration capacity of grout. However, bentonite affects the hydration of cement and lowers concrete strength [20]. Therefore, the mixing content of bentonite should be controlled in a certain range. Based on Liu [21], the percentage of bentonite is controlled at 5% in this paper to achieve an optimum improvement.

In addition, water over solid (W/S) ratio is controlled at 1.0 according to practical engineering. The volume ratios (VR) between cementitious suspensions and silicate are parametrically varied with 1:1, 2:1, 3:1 and 4:1. The specific proportion of mixture of experimental grout is shown in Table 3.

Table 3. Proportion of mixture of experimental grout

Number	VR	FA/%	PC/%	B/%
A1	1:1	20	75	5
A2	1:1	25	70	5
A3	1:1	30	65	5

B1	2:1	20	75	5
B2	2:1	25	70	5
B3	2:1	30	65	5
C1	3:1	20	75	5
C2	3:1	25	70	5
C3	3:1	30	65	5
D1	4:1	20	75	5
D2	4:1	25	70	5
D3	4:1	30	65	5

2.1.3 Testing procedure

Inverted cup tests are firstly carried out to measure the gelation time of the slurry under different fly ash content (FA) and volume ratio between cementitious suspensions and silicate (VR). Secondly, the specimens are produced in laboratory and the dimensions of the specimen are 40×40×160mm according to GB/T 17671-1999 [22]. The specimens are subsequently maintained in a standard curing room (23±3℃ and 100% R.H.) for 7 and 28 days, two maintenance conditions. Thirdly, a WDW-100E mechanical press is used to measure the flexural strength of the specimens with a speed of 2mm/min. Finally, Scanning Electron Microscope (SEM) photographs are investigated for assessing the anti-seepage properties in a micro perspective.

2.2 In-situ grouting test

2.2.1 Yellow River Silt

According to Cui [23], the Yellow River Silt consists of over 80% silt and a small amount of clay, with low surface strength, high porosity and drastic capillarity.

Prior to the in-situ tests, particle gradation test, direct shear test and permeability test are carried out. The test results of the particle gradation test and direct shear test are shown in Figs. 1 and 2 respectively. It can be seen that the particle gradation of the Yellow River Silt are relatively uniform and the particles in the size range 0.002mm - 0.074mm account for more than 80%. In addition, the gradation of the soil is poor, as C_u is smaller than 5. Based on the results from the direct shear tests, cohesion (c_q) and angle of shearing resistance (φ_q) are 10.78kPa and 23.67° respectively. The permeability of the Yellow River Silt is obtained by the variable water head permeability test and the tested permeability coefficient is 5.913×10^{-5}cm/s.
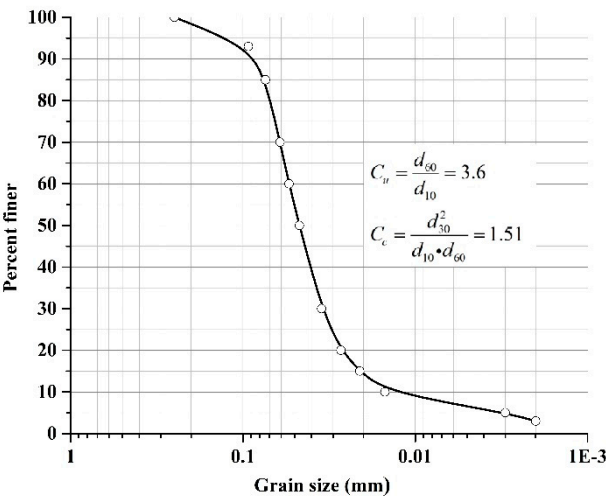

$$C_u = \frac{d_{60}}{d_{10}} = 3.6$$

$$C_c = \frac{d_{30}^2}{d_{10} \cdot d_{60}} = 1.51$$
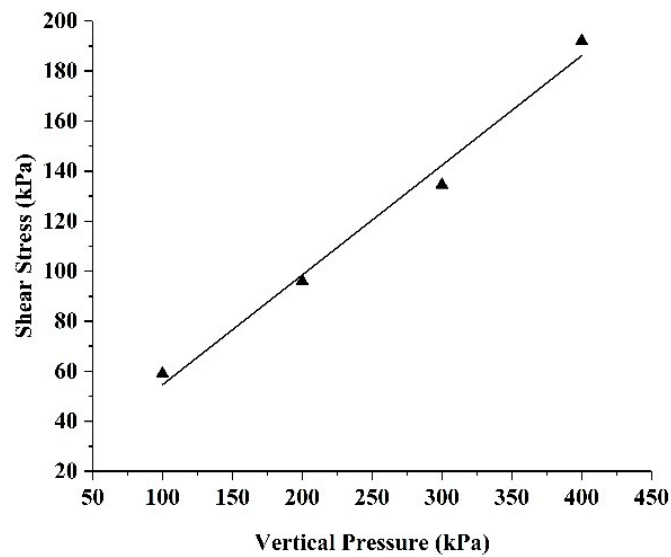
Fig 1. Particle size distribution curve

Fig 2. Result of direct shear test

2.2.2 Design of in-situ grouting tests

(1) Layout of grouting holes
The interval distance between grouting holes is determined by diffusion radius and grouting range, while diffusion radius is decided by rheological property of grouting material, grouting pressure and grouting time. However, there is a lack of theoretical relation for confirming the diffusion radius at present. As a consequence, the determination of the distance will be determined empirically based on practical applications.

When determining the interval distance, the lap effect between two holes should be taken into consideration. Based on the fact that the permeability of Yellow River Silt is relatively low, the fracture grouting would be the dominant type when conducting grouting experiment. According to the existing applications, the distance between two grouting holes can be determined as 1.0-2.0m. In order to further decide the optimum distance, the interval distance is parametrically varied from 0.8m to 1.5m in the tests. The layout of the grouting holes and the schematic cross section of the grouting field are shown in Fig. 3.
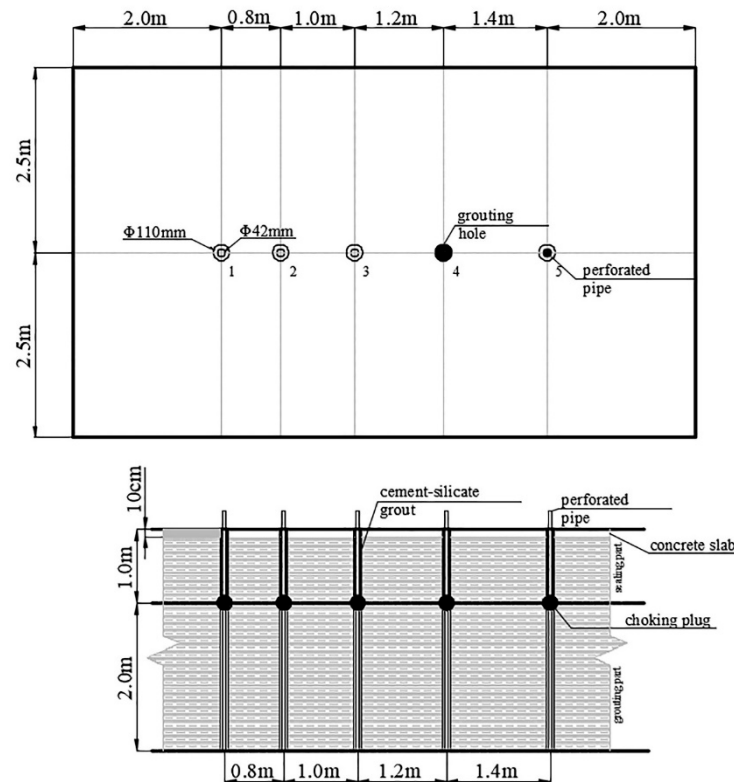
Fig 3. Layout of field test

(2) Grouting pressure

It is crucial to control the grouting pressure during the grouting process, which affects the compactness of the soil. However, deformation or even destruction of earth structures can occur when grouting pressure exceeds a critical value. Therefore, the grouting pressure should be controlled in a certain range. The maximum allowed value of fracture grouting pressure can be calculated by Eq. 1[24]

$$P_{max} = \gamma h + \sigma_t \tag{1}$$

Where γ, h andσ_t represent the specific weight of soil, the depth of grouting pipe and soil tensile strength respectively.

After substituting γ=15.5kN/m³, σ_t=10kPa(empirical value) and h=3m into Eq.1, the maximum allowable pressure is determined as 56.5kPa.

Considering that emitting slurry phenomenon may happen when grouting in shallow strata, the ultimate grouting pressure can be calculated by Eq.2 [25]

$$P_u \leq \gamma h \tan^2(45° + \varphi/2) + 2c \tan(45° + \varphi/2) \tag{2}$$

Based on the results in Section 2.2.1, the ultimate grouting pressure is calculated as 141.9kPa.

Combining the calculated results, initiation pressure and the ultimate pressure are determined as 60kPa and 150kPa in the field grouting experiment.

2.2.3 Grouting procedure

Perforated pipe grouting is used in in-situ tests. The grouting procedure involves grouting pad construction, positioning and drilling of grouting holes, preparation of the grout, and finally, injection of the grout. The flow chat of grouting is shown in Fig. 4a.

A concrete slab with dimensions of 8.4m×5m×10cm (length× width× depth) is produced as the grouting pad a week before the grouting injection. After fabricating the grouting pad for 3 days, the grouting holes are excavated according to Fig. 3. At the same time, the perforated pipes are produced with seamless steel tube with diameter of 48mm and wall thickness of 3.5mm. In order to generate directional grouting fractures along the axis, the hole distances on the pipe are designed to be different in two direction where one direction is 20cm and the other is 40cm. The direction of the dense holes on the pipes is marked with red oil paint. The detailed process is shown in Fig. 4b.

The optimum admixture content is obtained from the laboratory tests and is adopted in the in-situ tests. The cementitious suspensions and the water glass with Baume degree of 40 are placed in different agitated tanks. The prepared grout is agitated in case of sedimentation or setting. Meanwhile, drilling rig is used to bore the grouting holes according to the grouting holes positions.

After boring the grouting holes, perforated pipes are placed into the holes. It should be noted that the painted direction is parallel to the axial direction of the layout of the in-situ grouting test. Before injection, cement-silicate grout with volume ratio of 2:1 is used to seal the holes to avoid slurry inflow.

After preparation, the grout is pumped into the grouting holes and the sequence of grouting holes number is 1, 3, 5, 2 and 4. Thin slurry is used at the beginning and the grouting pressure increases progressively until it reaches the fracture pressure (about 0.06MPa). After spitting the soil, the grouting pressure is decreased and adjusted to the defined level. Meanwhile, the slurry is gradually densified. The injection process does not complete until one of the following two criteria is satisfied: either the volume of the injected grout is equal to the predefined volume (150-200kg/m) or the inflow injection pressure reaches the ultimate pressure (about 0.15MPa). When the injection completes, the circuits of the injection pump should be washed with clean water to avoid blocking. Besides, concentrated grout is injected to the grouting holes to seal the holes.
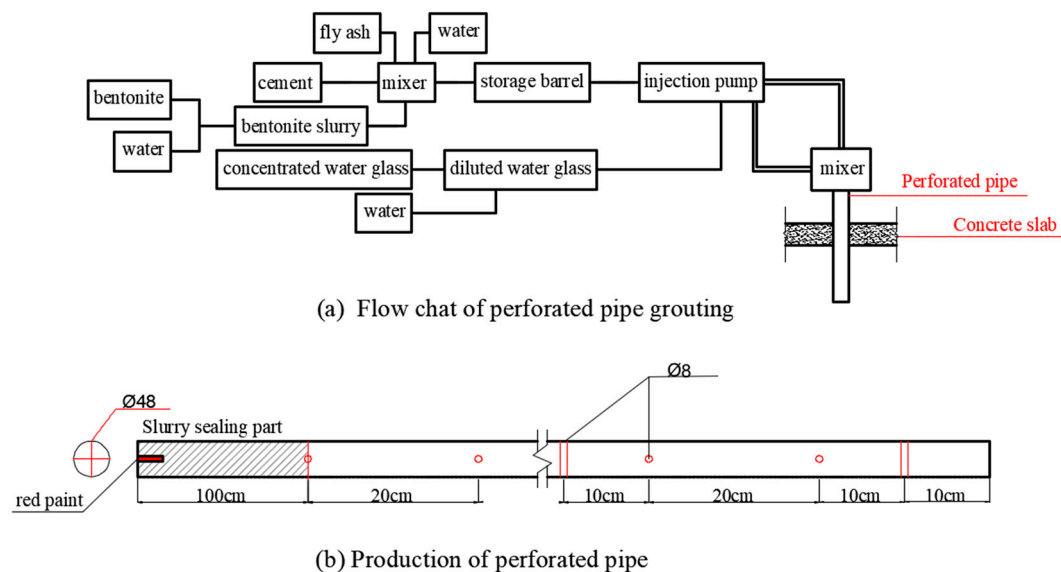

(a) Flow chat of perforated pipe grouting

(b) Production of perforated pipe

Fig 4. Flow chat of perforated pipe grouting and production of perforated pipe

2.2.4 Geophysical prospecting method

In order to comprehensively evaluate grouting effectiveness, both the Ground Penetrating Radar (GPR) and High Density Resistivity Method (HDRM) are used to avoid the limitation and multiplicity induced by a single method, as shown in Figs. 5 and 6. Pit prospecting is additionally carried out to investigate the reinforcement mechanism and the created grouting veins. The results of pit prospecting can verify the validity of the geophysical prospecting method and can further help to better understand the grouting mechanism in the soil.

The in-situ test procedure is described as follows. First, the reinforcement condition is detected using GPR and HDRM two weeks after grouting, where the layout of geophysical prospecting is

shown in Fig. 7. After geophysical prospecting, the grouted field is excavated to observe the grouting veins. Finally, part of the grouting veins is sampled, and the thickness of the grouting veins is measured.
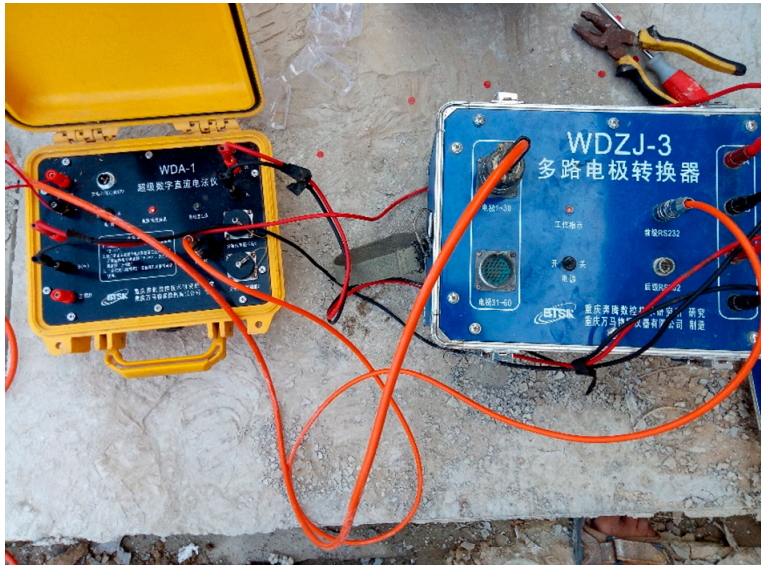

Fig 5. Ground Penetrating Radar
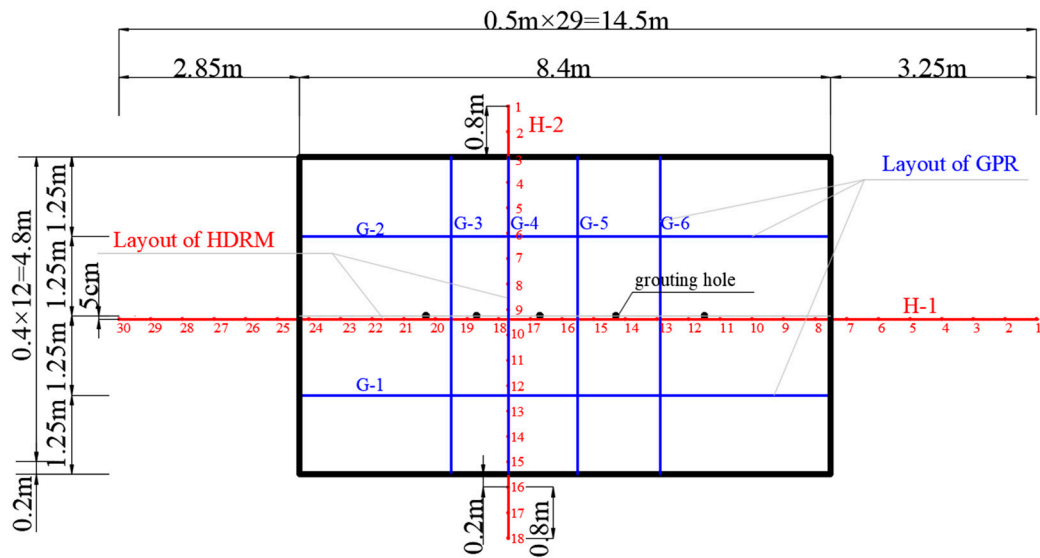

Fig 6. High Density Resistivity Method

Fig 7. The layout of GPR and HDRM

3 Discussion of laboratory results

3.1 Gelation time of the slurry

The test results in terms of gelation time of the slurry are shown in Fig. 8. The gelation time prolongs as fly ash content increases. When partly replacing cement with fly ash and bentonite, the water over cement ratio (W/C), that is a key factor in determining the setting time, decreases. In particular, the backfilled bentonite influences the hydration of cement and prolongs the gelation time. In practice, a slurry with appropriate gelation time is of great significance to avoid small range diffusion or water erosion. Therefore, the gelation time of slurry needs to be adjusted without greatly changing the slurry property by adding specific amount of fly ash.
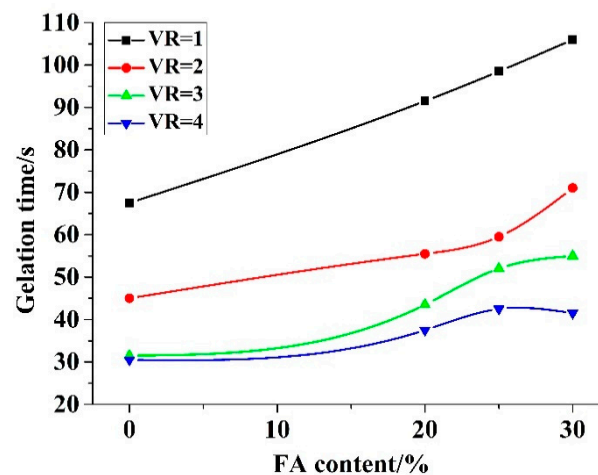

Fig 8. Test result of gelation time of the slurry

3.2 Strength of the specimen

The tested flexural strength of the specimens are shown in Fig. 9. Except for the case of 28-day maintenance and under the volume ratio of 1, all the other seven tests show that the flexural strength

increases and decreases as t fly ash content increases and reaches the peak when the fly ash content is in the range of approximately 25%.

W/C influences concrete strength as a result of the weakening effects from cement hydration when incorporating fly ash and bentonite. While backfilling 20% fly ash, pozzolanic reaction between fly ash and the hydrate of cement (such as calcium hydroxide) can increases concrete strength. In this case, fly ash is almost reacted and therefore its effect on improving the compactness of grout material is insignificant. When the percentage of fly ash increases to 25%, the hydration of fly ash further completes and the residual fly ash fills the pore in the concrete. Therefore, the flexural strength is higher than that of 20% fly ash. However, the residual fly ash is redundant and plays a negative role to the compactness. Therefore, the optimum range of fly ash is in the range of approximately 25% under the test condition.

Regarding the influence of volume ratio, when it is in the range of 2, the hydration action is relatively complete and the strength maximizes. After a threshold value of approximately 2, the volume ratio is so large that the silicate is not sufficient to react with hydration products (like calcium hydroxide), which eventually results in slightly decrease of the mechanical strength of the specimens.
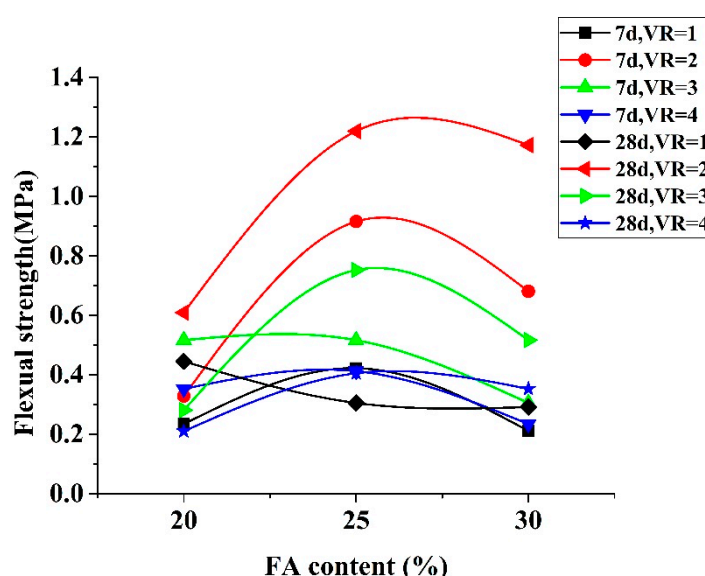

**Fig 9.** Test result of flexural strength of the specimen

3.3 SEM analysis of specimen

According to the test result in 3.1.1, the specimen B1, B2 and B3 are selected to investigate the influence of fly ash on the microstructure for the volume ratio of 2 using the scanning electron microscope (SEM). The photographs of SEM of the specimens under different fly ash are shown in Fig. 10.

Figs. 10a, 10c and 10e present the relatively low power field (50μm) of B1, B2 and B3 respectively. Figs. 10b, 10d and 10f present the relatively high power field (5μm) of B1, B2 and B3 respectively. According to Fig. 10e, it is noted that the pores in the concrete with 30% fly ash are large and numerous. It is presented in Fig. 10f that there is a large amount of fly ash in the surface of the microstructure. According to Fig. 10c, the compactness of the concrete significantly increases compared with Fig. 10e, and the micro-aggregate effect of fly ash is obvious with different sizes of fly ash particles embedded in the hydrates and those fly ash particles fill some void of the concrete. Furthermore, it is shown in Fig. 10d that a large amount of CSH form, which increases concrete strength. In Fig. 10a, there are more cracks and less fly ash particles on the surface of the concrete compared with the concrete under the fly ash percentage of 25%. The unreacted fly ash is insufficient and therefore the filling effect is not obvious as the microstructure in Fig. 10c.

Considering the results of mechanical strength and SEM, the macroscopic analysis and microscopic analysis show good agreements. In particular, the optimum mixing proportion of the

grout is 70% cement, 25% fly ash and 5% bentonite, and the best volume ratio is 2 for the investigated cases. The slurry under this mix proportion is selected for the subsequent in-situ grouting experiment.
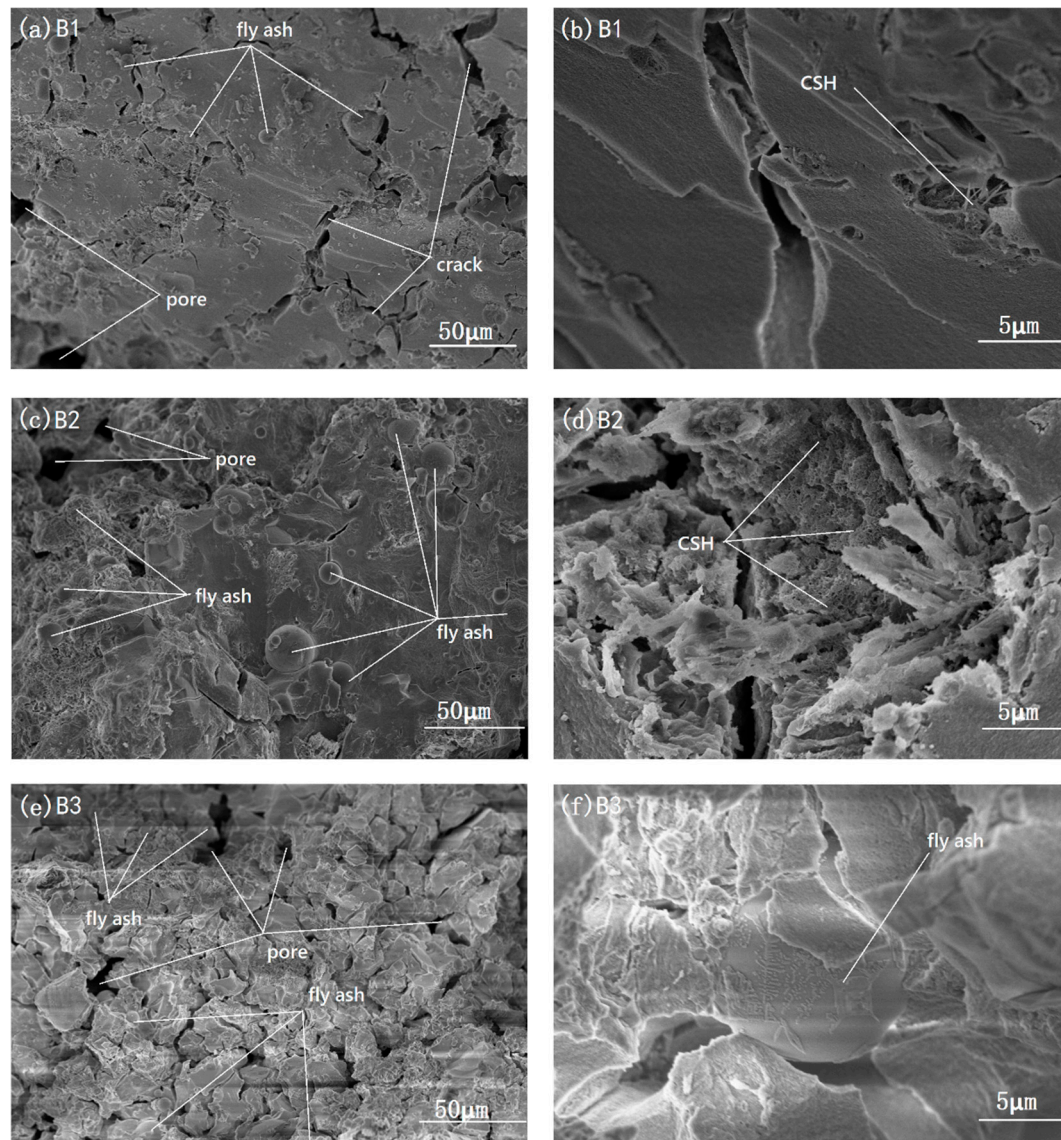
Fig 10. Photographs of SEM of the specimens under different fly ash content

4 Discussion of in-situ test results

Based on the obtained optimum admixture content, in-situ grouting tests are carried out in the Jinan Section of the Yellow River Embankment to evaluate the anti-seepage effectiveness of fracture grouting, where geophysical prospecting and pit prospecting methods are employed. In order to comprehensively discuss the grouting effectiveness, the geophysical prospecting results are divided into two parts: results in the axial direction and vertical direction.

4.1. Geophysical prospecting for grouting effectiveness

4.1.1 Results in axial direction

The results from the GPR and HDRM tests in the axial direction are shown in Figs. 11 and 12 respectively. According to Fig. 11, the soil in the grouting area can be divided into three layers, with the grouting slab and miscellaneous filling in the first layer, the unreinforced Yellow River Silt in the second layer and the strengthened silt in the third layer. The results show that there is continuous

inhomogeneous medium close to the grouting pipe, which is defined as the grouting vein. It is noted that there is obvious inhomogeneous medium near the pipes, numbered 3 and 4 in the upper of the excavation line.

Based on the prospecting results in Fig. 12, the distribution of resistivity includes three main horizontal layers in the grouting area. The first layer is high-resistance region with average thickness of 0.5m, which consists of low water content soil in the upper layer. The second layer is low-resistance area with the depth of 1.5m, without reinforcement. The third layer is a part with high resistivity compared with the second layer, where the overall water content is relatively low in this layer.

In summary, the grouting area can be divided into three layers and it shows good agreements with the actual grouting process. Regarding the grouting effectiveness, the mainly reinforcement area is the third layer where the water content is relatively low and there are grouting veins in the axial direction.
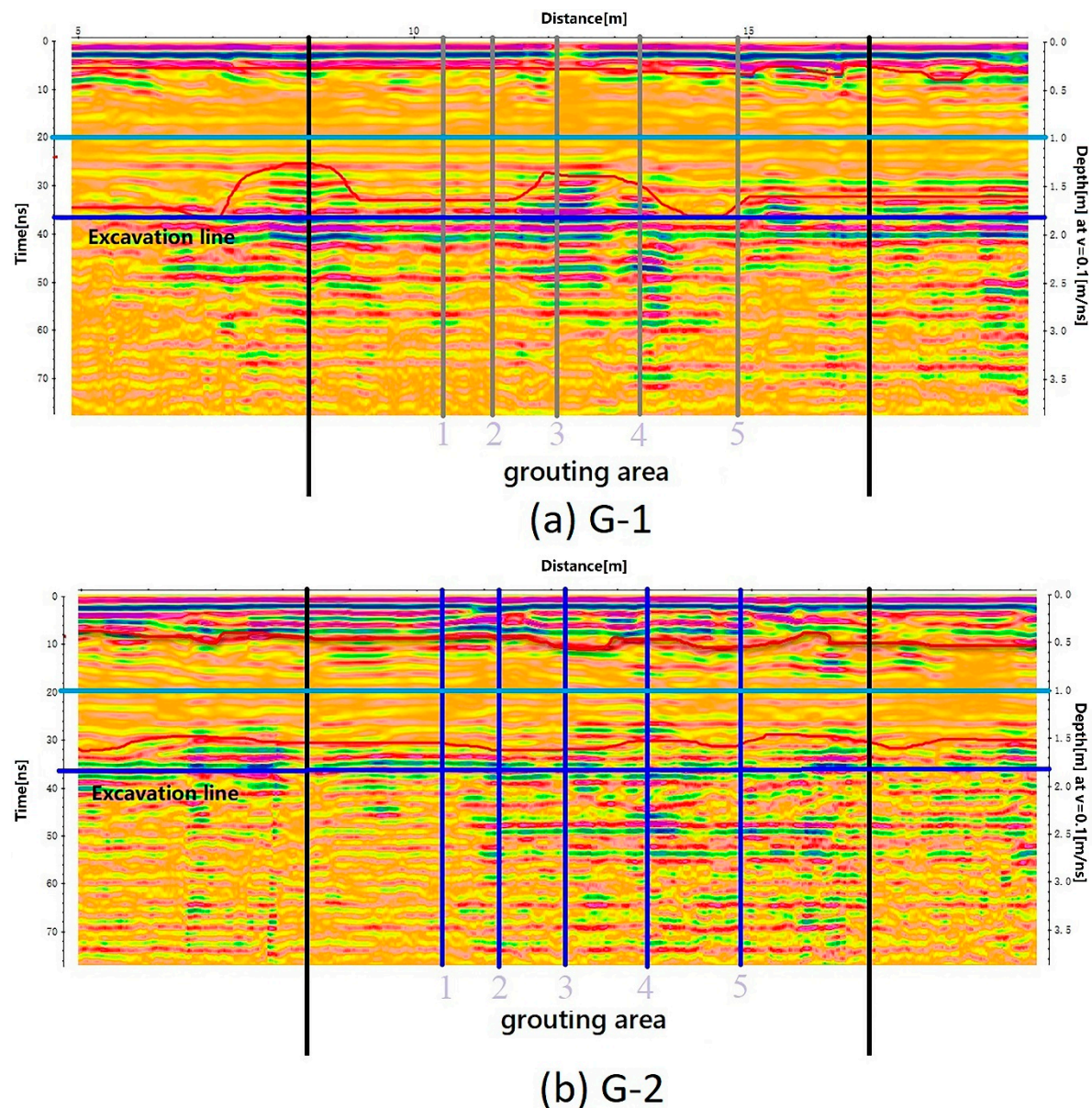

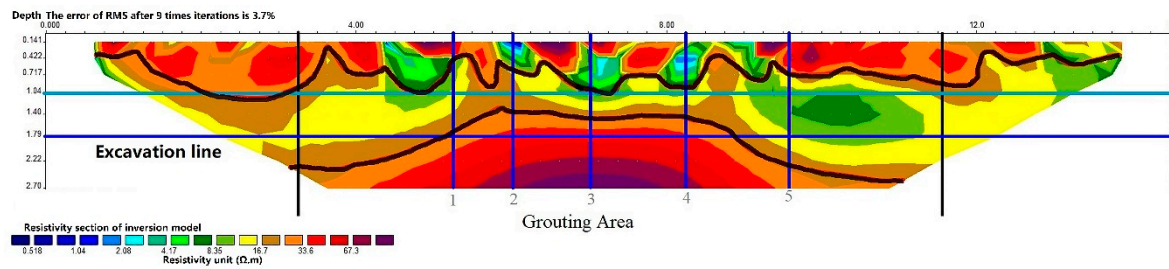**Fig 11.** Photographs of GPR in the axial direction

Fig 12. Photographs of HDRM in the axial direction

4.1.2 Vertical direction

The results from the GPR and HDRM tests in the vertical direction are presented in Figs. 13 and 14 respectively. Similarly, the soil can be divided into three layers according to Fig. 13. The depths of the first two layers are 0.30m and 1.65m respectively. The grouting materials are mainly found in the third layer. However, the grouting effectiveness is not as obviously observed as with the results in the axial direction, indicating that the grout mainly flows along the axial direction. Therefore, the treatment to the perforated pipe to induce the fracture direction is proved to be effective.

It is noted that the HDRM prospected depth in the vertical direction is only 1.91m. Fig. 14 shows that there are two layers in this range. The upper layer is a high-resistance area which is the grouting slab and miscellaneous filling. The lower part is a low-resistance region where there is no significant boundary in this layer in the depth of 1.5m, which indicates that the water content of the soil keeps unchanged. In other words, the grouting effectiveness is low.
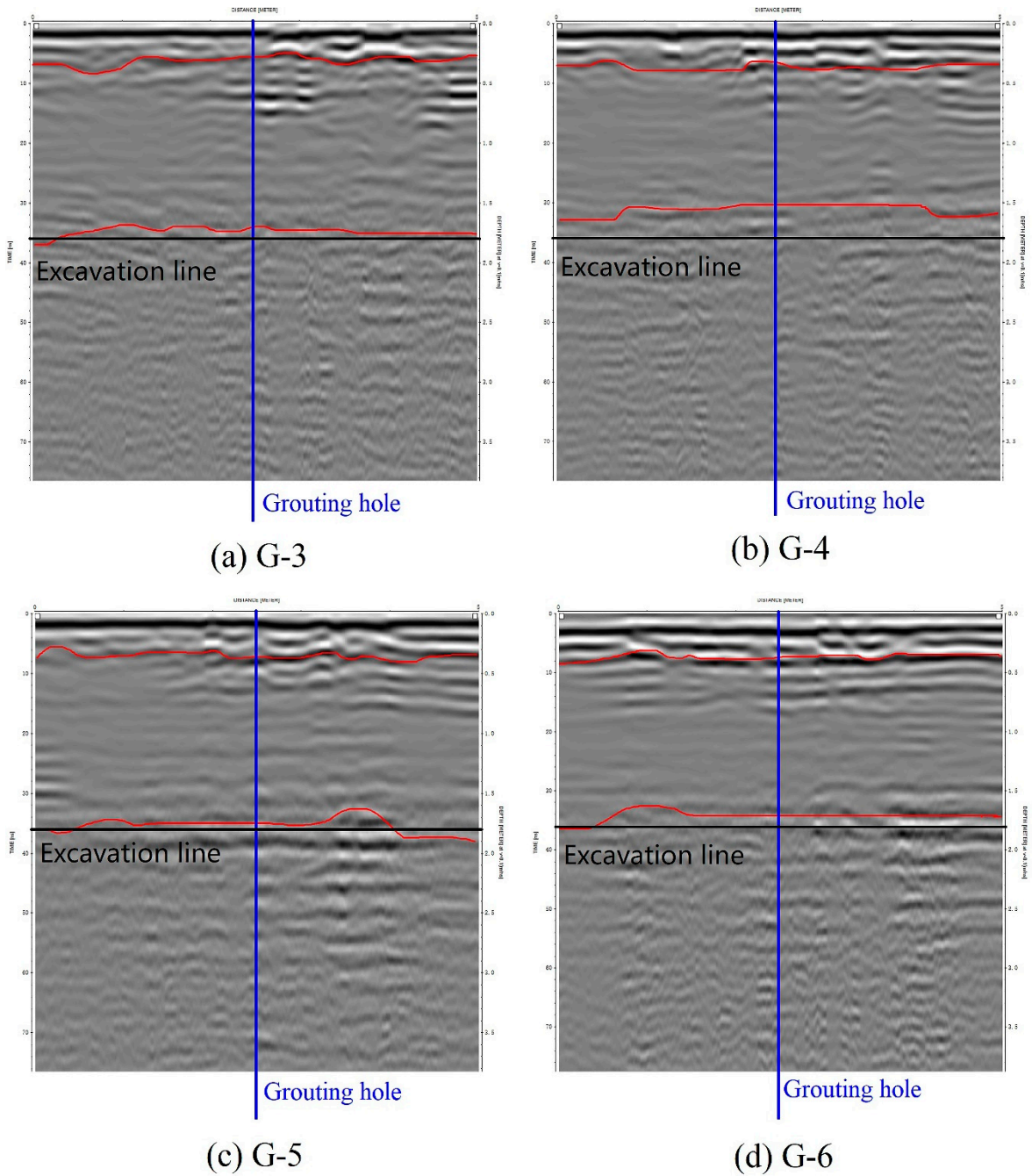
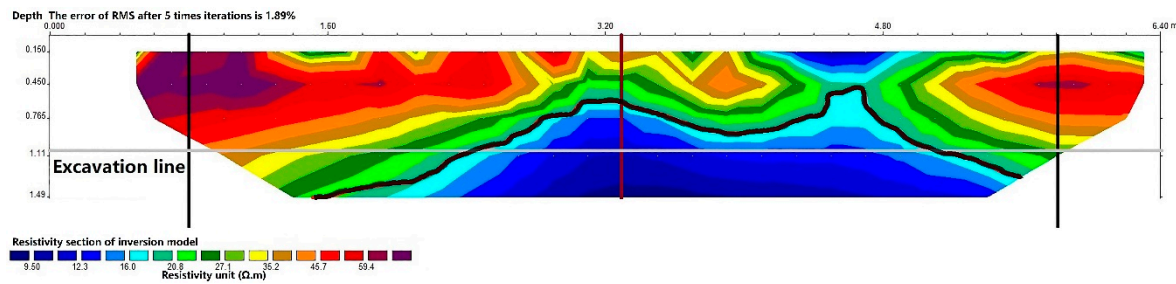**Fig 13.** Photographs of GPR in the vertical direction

Fig.14. Photographs of HDRM in the vertical direction

4.2 Pit prospecting for grouting effectiveness

The pit prospecting result is presented in Fig. 15. Considering that groundwater level is 1.27m and the mechanical strength of Yellow River silt is relatively low, the excavation depth is determined as 1.8m. In Fig. 15, the four color lines represent the grouting veins generated by grouting hole 2, 3, 4 and 5 respectively.

Based on Fig. 15, it can be seen that the grouting type in the Yellow River Embankment is fracture grouting. The grouting veins between the grouting hole 2 and 3 does not follow exactly the axial direction. The adjacent grouting overlaps at the vertical cross section of the grouting axis. When the interval distance of grouting holes is 1.2m, the grouting veins induced by the hole 3 and 4 laps and the thickness is relatively large, which indicates that the lap effectiveness is relatively satisfactory. When the grouting veins formed by grouting hole 5 laps with that of 4, it is evident that there is another grouting vein which is almost vertical to the axis. This is unfavorable to the reinforcement effect in generating anti-seepage curtain.
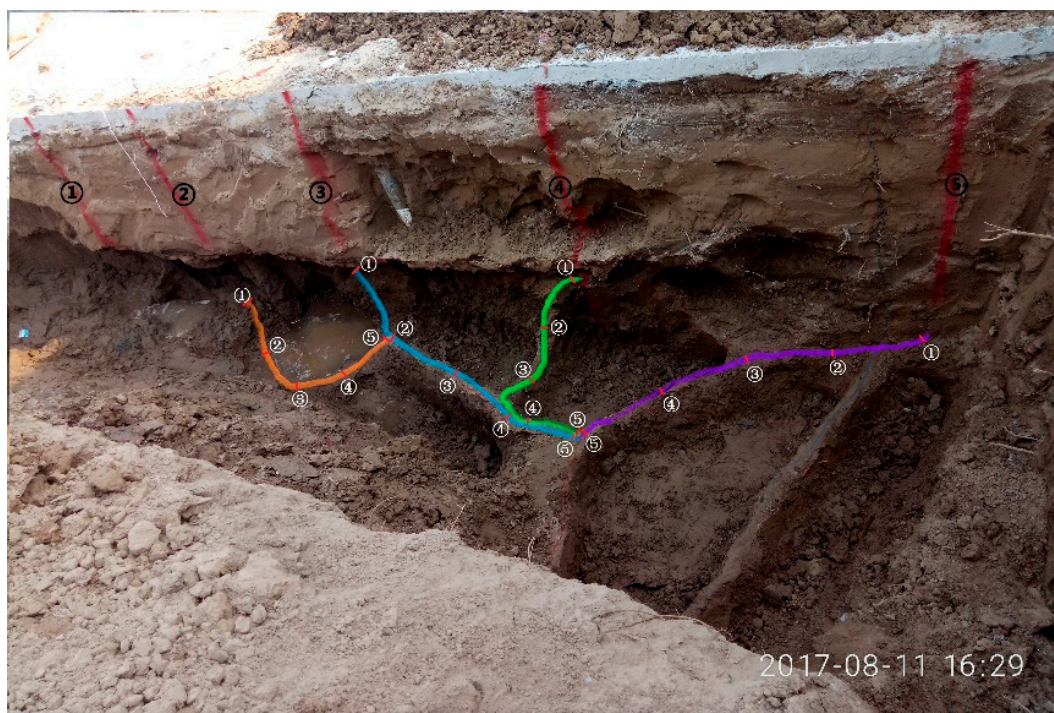
Fig 15. Pit prospecting result

In order to quantitatively investigate the grouting effectiveness, the grouting veins are sampled and the thickness of the veins is measured in laboratory. The test results are shown in Fig. 16. It can be seen that the four grouting veins overlap and form an anti-seepage curtain in the ground, showing satisfactory anti-seepage effects. The thickness of grouting veins reduces when it is further from the grouting hole. It is noted that the average thickness of the grouting vein induced by grouting hole 3 and 4 are relatively large, due to the appropriate grouting interval distance. After conducting permeability test for the grouting vein samples from grouting vein 3 and 4, the permeability coefficient is found to be 1.6×10^{-6}cm/s on average. According to DL/T 5129-2013, the required permeability coefficient for impervious body should be less than 1.0×10^{-5}cm/s. The modified cement silicate grouting material used in the in-situ tests can meet the anti-seepage criterion in practical engineering.
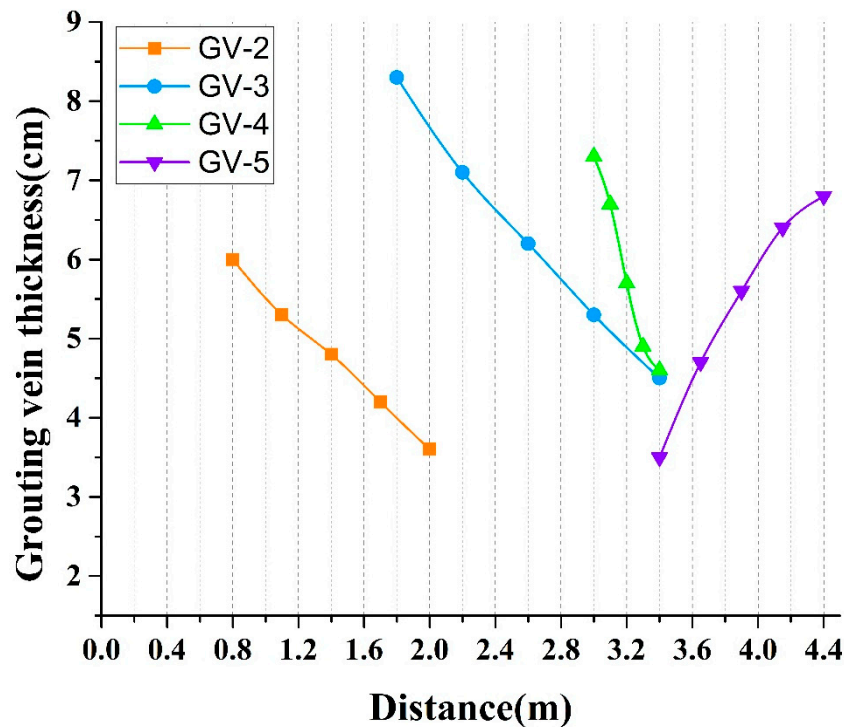
Fig 16. Measured value of the grouting veins

According to the pit prospecting result, it can be found that the pit test results show good agreements with the geophysical prospecting in the excavation range. The soil conditions within the excavation depth are well reflected by both the GPR and HDRM results. Therefore, the result of geophysical prospecting is reliable and the grouting effectiveness of the unexcavated part can be evaluated by geophysical prospecting. Moreover, when the interval hole distance is between 1.0m to 1.2m, the lap joint is relatively close to the grouting hole and the anti-seepage curtain can be easily controlled. When the interval distance is over 1.2m, some grouting veins are almost vertical to the reinforcement direction and they are unfavorable to the reinforcement effect in generating anti-seepage curtain. Therefore, the optimum interval hole distance should be in the range of 1.2m under the test conditions. After conducting permeability test for the grouting vein samples from grouting vein 3 and 4, the permeability coefficient is found to be 1.6×10^{-6}cm/s on average, which meets the anti-seepage criterion in practical engineering. In summary, the grouting type in Yellow River Silt is mainly fracture grouting. The grouting effectiveness of the field test is satisfactory based on the results of geophysical prospecting and pit prospecting tests.

5 Conclusions

In order to evaluate the anti-seepage effectiveness of fracture grouting employed in the Yellow River Embankment, laboratory and in-situ experiments were carried out for investigating the reinforcement effect of fracture grouting in the Jinan Section of the Yellow River Embankment. In particular, firstly, the laboratory tests concentrated on studying the optimum strength improvement for cement-silicate grout by varying the content of backfilled fly ash and bentonite as admixtures. Subsequently, in-situ grouting tests were carried out in the Jinan Section of the Yellow River Embankment to evaluate the anti-seepage effectiveness of fracture grouting, where geophysical prospecting and pit prospecting methods were employed. Based on the experimental results, the following conclusions can be drawn:

(1) Compared with pure cement-silicate grouts, the gelation time of the improved slurry is longer and gelation time increases as fly ash content increases. The optimum mixing proportion of

the compound cement-silicate grout is 70% cement, 25% fly ash and 5% bentonite, and the best volume ratio is 2 for the investigated cases.

(2) Good agreements are shown between the Ground Penetrating Radar and High Density Resistivity methods and the two geophysical prospecting methods can both reflect the anti-seepage effectiveness of fracture grouting on site.

(3) The pit prospecting result shows that grouting material mainly flows along the axial direction of the embankment, which means that the treatment used to generate directional fracture is proved to be effective. The injection hole interval distance is suggested to be 1.2m, where the lapping effect of the grouting veins is relatively significant.

(4) For the investigated cases, the average thickness of the grouting veins is approximately 6.0cm and the corresponding permeability coefficient is averagely 1.6×10^{-6}cm/s, which meets the anti-seepage criterion in practice.

Acknowledges

References

1. Jorne, F.; Henriques, F. M. A. Evaluation of the grout injectability and types of resistance to grout flow. *Construction & Building Materials* **2016**, *122*, 171-183, https://doi.org/10.1016/j.conbuildmat.2016.06.032.

2. Azadi, M. R.; Taghichian, A.; Taheri, A. Optimization of cement-based grouts using chemical additives. *Journal of Rock Mechanics and Geotechnical Engineering* **2017**, 9, 623-637, https://doi.org/10.1016/j.jrmge.2016.11.013.

3. Pasian, L.; Secco, M.; Piqué, F.; Artioli, G.; Rickerby, S.; Cather, S. Lime-based injection grouts with reduced water content: An assessment of the effects of the water-reducing agents ovalbumin and ethanol on the mineralogical evolution and properties of grouts. *Journal of Cultural Heritage* **2018**, *30*, 70-80, https://doi.org/10.1016/j.culher.2017.10.003.

4. Warner, J.; Jefferies, M.; Garner, S. Compaction Grouting for Sinkhole Repair at WAC Bennett Dam. *International Conference on Grouting and Ground Treatment* **2003**, 869-880, https://doi.org/10.1061/40663(2003)21.

5. Grotenhuis, R. Fracture grouting in theory, MD Thesis, Delft University of Technology, Netherlands. 2004.

6. Tunçdemir, F.; Ergun, M. U. A Laboratory Study into Fracture Grouting of Fissured Ankara Clay. *Geo-Frontiers Congress* **2005**, 1-12, https://doi.org/10.1061/40783(162)16.

7. Bezuijen, A.; Grotenhuis, R. T.; Tol, A. F. V.; Bosch, J. W.; Haasnoot, J. K. Analytical model for fracture grouting in sand. *Journal of Geotechnical & Geoenvironmenta Engineering* **2011**, 137, 611-620, https://doi.org/10.1061/(asce)gt.1943-5606.0000465.

8. Yoneyama, K.; Okuno, T.; Nakaya, A.; Tosaka, H. Experimental and numerical study on fracture grouting by fine particle cement. Chemistry Letters **2012**, 1994, 9-12.

9. Yun, J. W.; Park, J. J.; Kwon, Y. S.; Kim, B. K.; Lee, I. M.. Cement-based fracture grouting phenomenon of weathered granite soil. *KSCE Journal of Civil Engineering* **2016**, 21, 1-11, https://doi.org/10.1007/s12205-016-0862-1.

10. Wang, Q.; Wang, S., Sloan, S. W.; Sheng, D.; Pakzad, R. Experimental investigation of pressure grouting in sand. *Soils & Foundations* **2016**, 56, 161-173, https://doi.org/10.1016/j.sandf.2016.02.001.

11. Sun, F.; Zhang, D. L.; Chen, T. L; Zhang, X. P. Meso-mechanical simulation of fracture grouting in soil. *Chinese Journal of Geotechnical Engineering* **2010**, *32*, 474-480.

12. Liu, Q.; Zheng, X. L.; Liu, H. J.; Wang, J. G.; Dong, S. Y. Experimental studies on liquefaction behavior of silt in the huanghe river delta. *World Earthquake Engineering* **2007**, 23, 161-166. 10.3969/j.issn.1007-6069.2007.02.026.

13. Xiao, J., Liu, J., Peng, L., & Chen, L. Effects of compactness and water yellow-river alluvial silt content on its mechanical behaviors. *Rock & Soil Mechanics* **2008**, 29, 409-414. 10.3969/j.issn.1000-7598.2008.02.022.

14. Song, X. G.; Zhang, H. B.; Wang, S. G.; Jia, Z. X.; Guan, Y. H. Hydrophilic characteristics and strength decay of silt roadbed in yellow river alluvial plain. *Chinese Journal of Geotechnical Engineering* **2010**, 32.1594-1602.

15. Zhu, D. Y., Guan, Y. H., Liu, H. Z., Wang, Q., & Zhang, Q. T.. Model tests on fracture grouting reinforcement of silt embankment by using soletanche method. *Chinese Journal of Geotechnical Engineering* **2012**, 34, 1425-1431.

16. Chen, C. L., Ma, S. X., Li, L. L., & Cai, Z. P. Study on post-cyclic undrained deformation and strength characteristics of saturated silt in the floodplain of the yellow river. *Journal of Hydraulic Engineering* **2014**, 45, 801-808. 10.13243/j.cnki.slxb.2014.07.006.

17. Shi, M. S.; Xia, W. Y.; W, F. M.; L, H.; Pan, Y. H.). Experimental study on bond performance between polymer anchorage body and silt. *Chinese Journal of Geotechnical Engineering* **2014**, *36*, 724-730.

18. ASTM C618-05, *Standard Specification for Coal Fly Ash and Raw or Calcined Natural Pozzolan for Use in Concrete* **2005**, West Conshohocken, PA

19. Sha, F.; Li, S.; Liu, R.; Li, Z.; Zhang, Q. Experimental study on performance of cement-based grouts admixed with fly ash, bentonite, superplasticizer and water glass. *Construction & Building Materials* **2018**, *161*, 282-291. https://doi.org/10.1016/j.conbuildmat.2017.11.034

20. Hwang, H.; Yoon, J., Rugg, D.; Mohtar, C. S. E. Hydraulic Conductivity of Bentonite Grouted Sand. *Geo-Frontiers Congress* **2011**, 1372-1381. https://doi.org/10.1061/41165(397)141

21. Liu, J.; Hu, L. Q.; Xu, B. J.; Yue, X. L.; Qi, B. L.; Zhong, Q. Study on cement-based seepage grouting materials for earth-rock dam. *Journal of Shandong University (engineering science)* **2016**, *47*, 9-15

22. Chinese National Quality and Technical Supervision & Chinese Ministry of Construction; *Method of testing cements-Determination of strength*, Standards Press of China: Beijing, China, 1999; pp. 1-12.

23. Cui, X. Traffic-induced settlement of subgrade of low liquid limit silt in yellow river delta. *China Civil Engineering Journal* **2012**, *45*, 154-162.

24. National Development and Reform Commission of the People's Republic of China; *Technical specification of grouting for earth dam*, China Water & Power Press: Beijing, China, 2010; pp. 1-18.

25. Collaboration of Rock and Soil Grouting Theory and Engineering Examples; *Rock and Soil Grouting Theory and Engineering Examples*. Science Press: Beijing, China, 2001; pp. 71-94.